The International Journal of Cardiovascular Imaging (2019) 35:1509–1524
https://doi.org/10.1007/s10554-019-01615-8

ORIGINAL PAPER

State of the art: utility of multi-energy CT in the evaluation of pulmonary vasculature

Prabhakar Rajiah[1] · Yuki Tanabe[1,2] · Sasan Partovi[3] · Alastair Moore[4]

Received: 26 February 2019 / Accepted: 25 April 2019 / Published online: 2 May 2019

Abstract

Multi-energy computed tomography (MECT) refers to acquisition of CT data at multiple energy levels (typically two levels) using different technologies such as dual-source, dual-layer and rapid tube voltage switching. In addition to conventional/routine diagnostic images, MECT provides additional image sets including iodine maps, virtual non-contrast images, and virtual monoenergetic images. These image sets provide tissue/material characterization beyond what is possible with conventional CT. MECT provides invaluable additional information in the evaluation of pulmonary vasculature, primarily by the assessment of pulmonary perfusion. This functional information provided by the MECT is complementary to the morphological information from a conventional CT angiography. In this article, we review the technique and applications of MECT in the evaluation of pulmonary vasculature.

Keywords CT · Dual-energy CT · Multienergy CT · CT perfusion · Pulmonary embolism

Introduction

Multi-energy CT (MECT) or spectral CT refers to the acquisition of CT data at multiple different energy levels. Practically, this involves acquisition at two energy levels, and hence, this is commonly called dual-energy CT (DECT). Tissues and materials show different attenuation properties at different energy levels. At low energy levels, photoelectric effect is the predominant interaction and is dependent on the atomic number. At high energy levels, Compton effect predominates and is dependent on tissue density. Most of the tissues and materials can be expressed as a linear combination of several basic material densities, such as water, soft tissue, fat, and iodine. This differential attenuation at different energy levels can distinguish tissues and materials beyond a conventional CT, which relies only on densities [1].

Dual source, rapid tube-voltage (kVp) switching and dual-layer are the most commonly used MECT technologies (Fig. 1). In the dual-source technology, there are two x-ray tubes that are located 90° from each other that can be operated at two different energy levels (Fig. 1a). In the rapid kVp switching technology, the tube voltage is switched between high and low energies for each x-ray projection (Fig. 1b), and there is a highly-responsive gemstone scintillator detector system. In the dual-layer detector-based spectral technology, there is a single x-ray tube, but there are two layers in the x-ray detector. The top layer absorbs the low energies, and the bottom layer absorbs high energies (Fig. 1c) [2]. Dual-spin and split-beam are less commonly used technologies. All of these scanners, with the exception of dual-layer CT can be operated either in the single or dual-energy mode and the decision to operate in a dual-energy mode should be prospectively made. With the dual-layer CT, there is no need for this prospective selection, since all the patients scanned using this technology will have dual-energy data available, which can be retrospectively reconstructed on demand. Photon counting CT is an experimental technology in which more than two energy levels can be separated.

✉ Prabhakar Rajiah
radpr73@gmail.com

1 Cardiothoracic Imaging Division, Department of Radiology, University of Texas Southwestern Medical Center, E6.122G, 5323 Harry Hines Boulevard, Mail Code 9316, Dallas, TX 75390-8896, USA

2 Ehime University Graduate School of Medicine, Ehime, Japan

3 Interventional Radiology Section, Imaging Institute, Cleveland Clinic Foundation, Cleveland, OH, USA

4 Department of Radiology, Baylor University Medical Center, Dallas, TX, USA

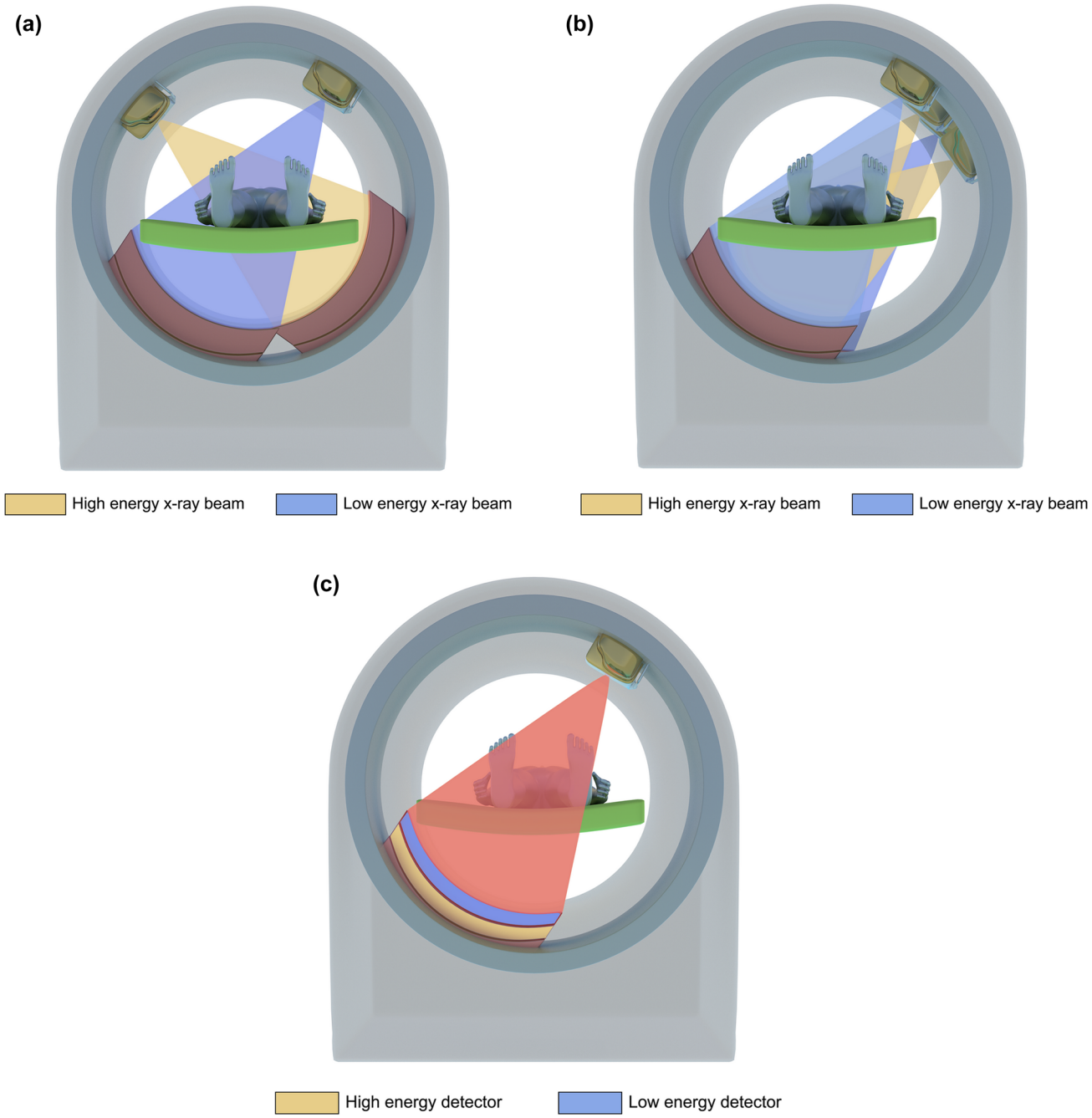

Fig. 1 Multienergy CT technologies. **a** Dual source technology has two x-ray tubes that are located 90° to each other, and operated at different tube voltages. **b** Rapid kVp switching technology has a single x-ray tube, but the tube voltage is rapidly switched for each x-ray projection between high and low energies. **c** Dual layer technology has a single x-ray tube but has two layers of x-ray detectors, with the top layer absorbing low energy photons and the bottom layer absorbing high energy photons

In this article, we review the technique and applications of MECT in the evaluation of pulmonary vasculature.

MECT post-processing and image types

MECT technology generates routine diagnostic images similar to a conventional CT scan (Fig. 2a). In the dual source and rapid kVp switching technologies, these are obtained by mixing the low and high energy images at

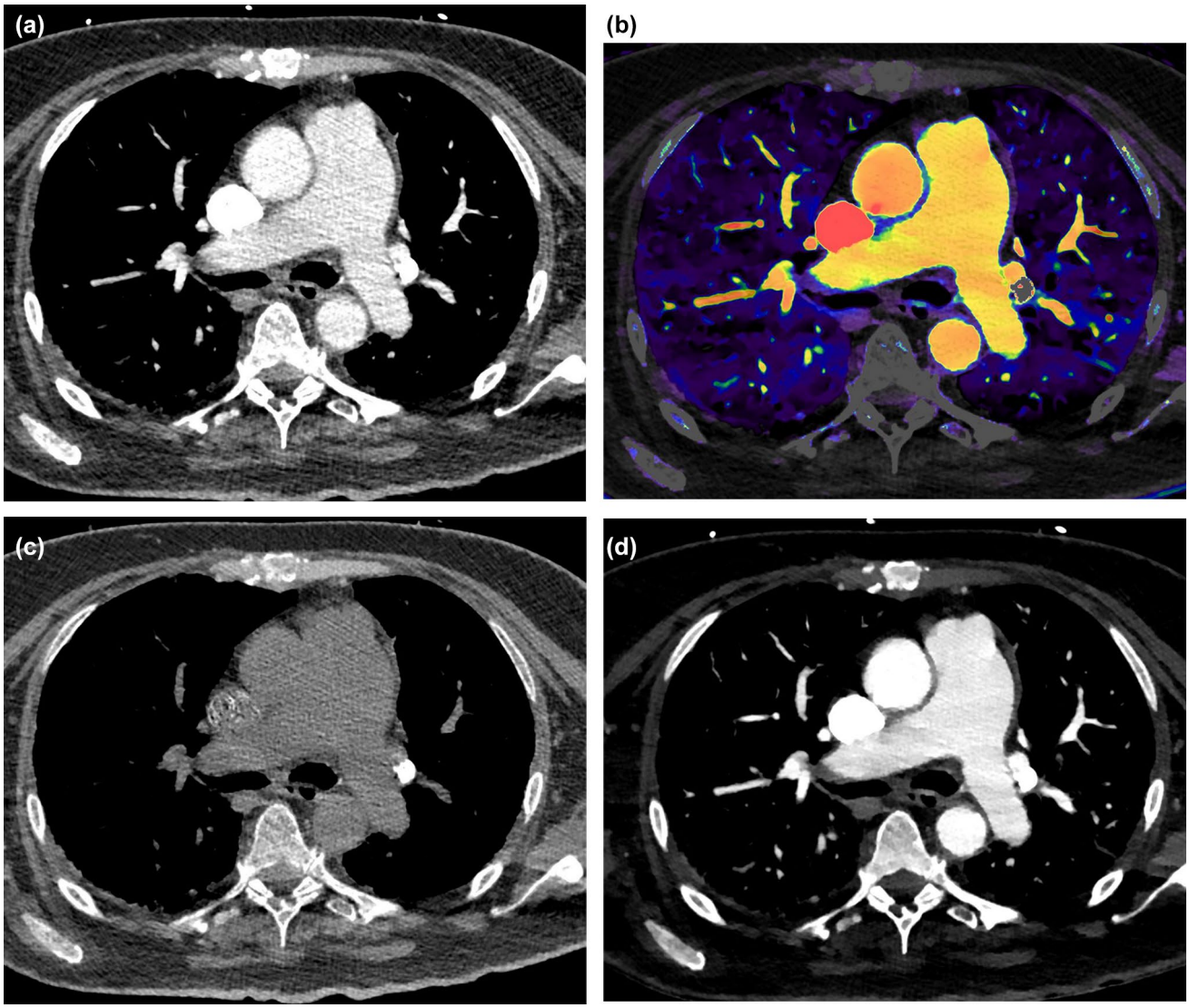

Fig. 2 Multienergy CT images. **a** Conventional/routine diagnostic image from a dual-layer CT scanner mimics the images that are routinely used for diagnosis in a single-energy CT scanner. In this technology, these images are generated from al the x-ray data that is incident on the two layers of detectors combined. **b** Iodine map image which highlights tissues containing iodine, can be fused on morphological images. **c** Virtual non contrast (VNC) image in which the pixels containing iodine are removed, and hence the image resembles a non-contrast CT image. **d** Virtual monoenergetic image (VMI), which mimics an image that is obtained using a single energy x-ray. This can be generated from 40 keV to 200 keV. Here is an example of VMI at 40 keV in which the signal from contrast is bright

different proportions (typically, 30% of low energy and 70% of high energy data). Conversely, in the dual-layer system, these are derived by utilizing all the x-ray data that is incident on the detectors (both top and bottom layers) [1, 2]. MECT also provides multiple additional unique image sets by a process of two or three-material decomposition, which can distinguish tissues that are expressed as a linear combination of basic material densities. Since the attenuation coefficients of different materials at different energies are known, by estimating the attenuation of each voxel at low and high energies, the contribution of two or three specific materials to the voxel attenuation can be estimated [3]. Specific tissues or materials can be highlighted or removed from images. For example, a three material decomposition of iodine, soft tissue, and air can be used to generate iodine maps (Fig. 2b) and virtual non-contrast (VNC) images (Fig. 2c). Iodine maps highlight tissues containing iodine, and VNC images, in which pixels containing iodine are removed, mimick a true non-contrast image. Both of these imagesets are useful in lesion characterization. Iodine maps are also useful in the evaluation of perfusion. Virtual monoenergetic images (VMI) mimic x-ray beams of a single energy level and are obtained by the linear combination of basis pair images

(i.e. low and high energy or photoelectric and Compton images) at different proportions (Fig. 2d). VMI at 70 keV is considered the equivalent of a conventional 120 kVp polyenergetic image, with similar attenuation values. At lower energy VMIs (< 70 keV), the signal of contrast increases, since these energies approximate the K-edge of iodine, resulting in higher photoelectric attenuation. At higher energy levels (> 70 keV), the signal of contrast progressively decreases, but image artifacts such as beam hardening are typically lower [1, 2]. Other less commonly used image types are available including effective atomic number, electron density, and uric acid pair images [1].

Iodine maps are the most commonly used MECT images in the evaluation of pulmonary vasculature and provide qualitative and quantitative information on pulmonary perfusion. For obtaining good quality MECT perfusion images from a CT pulmonary angiography (CTPA), a higher concentration of iodine (> 300 mg/ml) and a slightly longer scan delay (4–7 s) are used to distinguish iodine in the lung and allow optimal contrast distribution in lung parenchyma [4]. A pulmonary perfused blood volume (PBV) is a color coded map of iodine concentration (typically a 16-bit-color scale). The analysis of the iodine concentration in PBV map is restricted to the lung parenchyma using a threshold-based algorithm based on CT attenuation (for example, default − 960 to − 600 HU) (Fig. 3) [5, 6]. Perfusion defects are color coded and can be normalized to the vascular iodine concentration. Structures outside this attenuation range are excluded from analysis, and hence lung abnormalities outside this range will appear dark. The PBV map can be fused with a conventional CT image, allowing comprehensive assessment of morphological and functional information on the same images [7, 8]. Three-dimensional (3D) maps similar to a scintigraphic perfusion image can also be generated (Fig. 3b).

By definition, perfusion is the volume of blood flowing through a cubic centimeter of tissue per second [9, 10] and typically requires dynamic CT acquisition of different timepoints, using a high volume of contrast at a high flow rate. Hence, MECT perfusion images are not true perfusion images but rather reflect the enhancement at a single point of time. However, one can consider the scan a two time-point acquisition by considering the inherent physical density of image as the first time point and acquisition time as the second time point [3]. Despite this technicality, MECT-perfusion is a good surrogate for lung perfusion, since it has been shown that the enhancement values increase with volume of contrast material [11]. It is also acquired without changing the CTA protocol and does not suffer from a radiation dose penalty or misregistration from multiple acquisitions [3]. MECT perfusion images are comparable to and show high correlation with scintigraphic perfusion images despite their differing physiological mechanisms and their acquisitions at different phases of breathing (inspiration for MECT and shallow breathing for V/Q scan). One study showed 99% specificity and 83% sensitivity of MECT compared with planar V/Q scans at a segmental level [12], while another study showed 76% specificity and 96% sensitivity compared with SPECT [13].

The generation of these additional MECT images can either be done on a dedicated post-processing workstation by the radiologist on a per-case basis or a pre-determined set of MECT images can be automatically/manually generated at the scanner depending on the specific clinical protocol [1]. For example, for a PE protocol, PBV maps in multiple planes, VMI at 40 keV and VNC image can be automatically generated. The creation of additional MECT images will

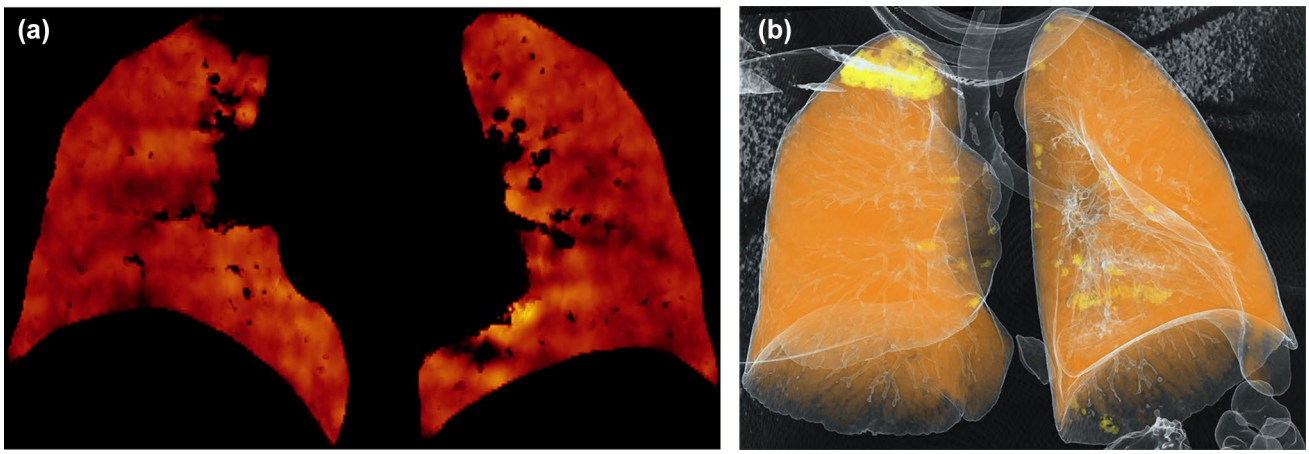

Fig. 3 MECT perfusion of lungs. **a** Pulmonary blood volume (PBV) map in which a threshold algorithm of CT attenuation is used to restrict the analysis of iodine concentration to the lung parenchyma. Normally perfused lung is color coded as orange and perfusion defects will be seen as dark areas. **b** 3D volume rendered lung perfusion image which resembles a scintigraphic perfusion image

cost some additional time at the scanner, usually in the range of 5–10 min. Multiple additional imagesets are available in PACS, which might be a concern if there are storage limits. Although, there were initial concerns that radiation dose is higher with MECT, they are typically radiation-dose neutral with appropriate protocols [1]. However, it should be noted that with the dual-source scanner, there is also a high-pitch helical mode available in the latest generation scanners, which provides images with lower motion, radiation and contrast doses, but no MECT images [1]. The appropriate mode, i.e. high-pitch helical versus MECT mode should be judiciously selected based on the clinical indication.

Clinical applications of MECT in pulmonary vasculature

The most common clinical application of MECT in pulmonary vasculature is for the evaluation of acute pulmonary embolism, chronic pulmonary embolism, and pulmonary hypertension (PH) (Table 1).

Acute pulmonary embolism

Acute pulmonary embolism, a potentially life threatening emergency, is diagnosed with high accuracy (pooled sensitivity of 82%, pooled specificity of 94.9%) using CTPA [14]. Direct findings of acute PE in CTPA include a filling defect in the vessel surrounded by contrast material, an eccentric filling defect that makes an acute angle with the vessel wall, or complete occlusion of a dilated vessel [15]. CT also provides risk stratification by metrics such as clot burden and right heart strain (right ventricular enlargement, ventricular septal flattening, reflux of contrast into the IVC and hepatic veins). MECT provides complementary information and has incremental benefits in the evaluation of acute PE. For example, the detection of acute PE can be improved with vascular mapping by color-coding the vessels based on the iodine concentration, either with 2D or 3D reformats. Color coding enables easy distinction of vessels with no iodine concentration from those with iodine concentration (Fig. 4). This has high negative predictive value for excluding segmental PE and can distinguish PE from flow artifacts and partial volume averaging [16].

A wedge-shaped perfusion defect in a segmental, subsegmental, or lobar distribution is a feature of acute PE in MECT (Fig. 5). Visual assessment of this perfusion defect has high accuracy compared to CTA as a reference standard with high sensitivity (85%) and specificity (96%) [17]. Accuracy is higher on a per-patient than per-segment basis. One study showing 100% sensitivity and specificity on a per-patient basis with 60–66.7% sensitivity and 99.5 to 99.8% on a per-segment basis [18]. Another study showed 75% sensitivity and 80% specificity on a per-patient basis and 83% sensitivity and 99% specificity on a per-segment basis [19]. In a rabbit study that used

Table 1 Clinical applications of multienergy CT in the pulmonary vasculature in addition to the morphological information provided by conventional CT

Clinical applications	Findings	Utility	Useful images
Acute pulmonary embolism	Wedge shaped perfusion defect in segmental or sub-segmental distribution	Increases sensitivity for the detection of PE, especially segmental and subsegmental Severity, risk stratification and prognosis Monitoring response to therapy Salvaging suboptimal studies and low contrast dose Decreasing artifacts such as beam hardening	Perfusion maps Virtual monoenergetic Virtual non contrast
Chronic pulmonary embolism	Perfusion defects- usually well defined, large, multiple segmental or subsegmental, wedge/mottled/mosaic	Establishing the diagnosis Determining the severity Selecting patients suitable for surgery/intervention Monitoring response to therapy	Perfusion maps Virtual monoenergetic
Pulmonary hypertension	Perfusion defects—heterogeneous, small, non-segmental; wedge/mosaic/mottled	Determining severity, risk stratification, prognosis Non invasive hemodynamics Monitoring response to therapy	Perfusion maps Virtual monoenergetic Virtual non contrast
Miscellaneous Congenital Neoplasm Vasculitis	Congenital—perfusion abnormalities in interruption/atresia Neoplasm—perfusion in patients with tumor emboli Vasculitis—perfusion defect in lung	Establishing diagnosis Determining severity	Perfusion maps

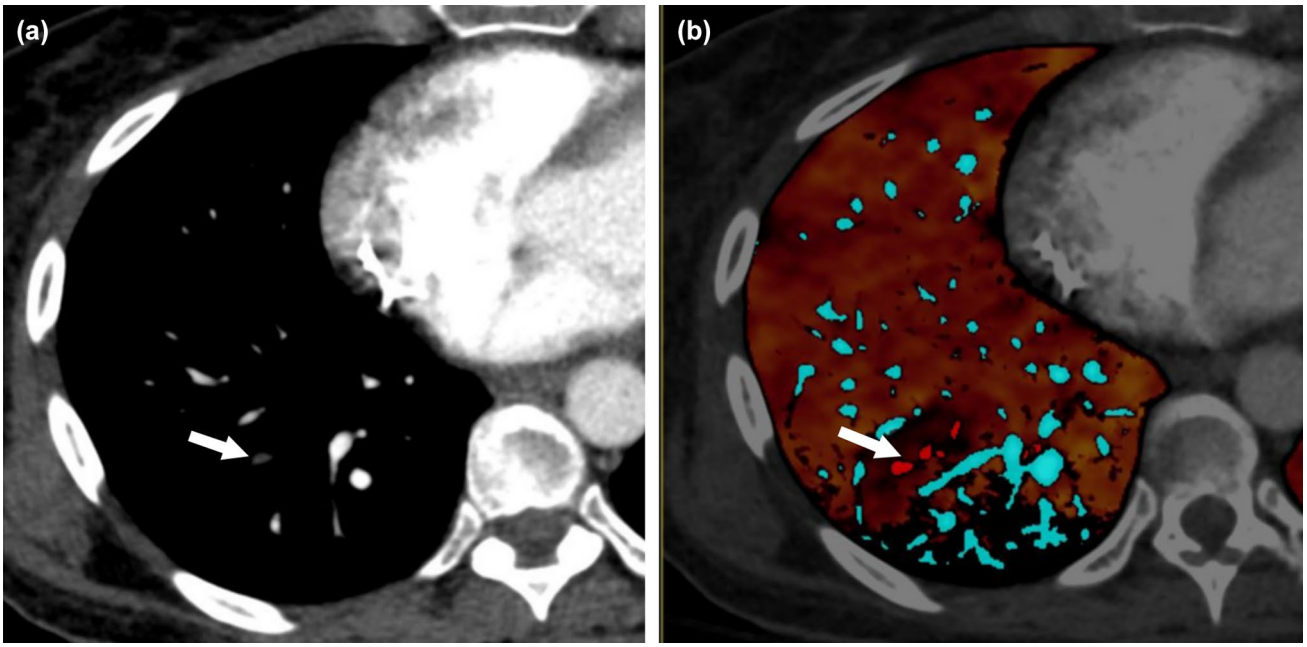

Fig. 4 Dual-energy color coding of vessels. **a** Conventional CTA shows subtle clot in posterior segmental branch of the right lower lobe (arrow). **b** Dual-energy color coded images based on iodine concentration shows the vessel containing clot as red color (arrow) due to absent/low iodine concentration, whereas normal iodine containing vessels are coded in blue color

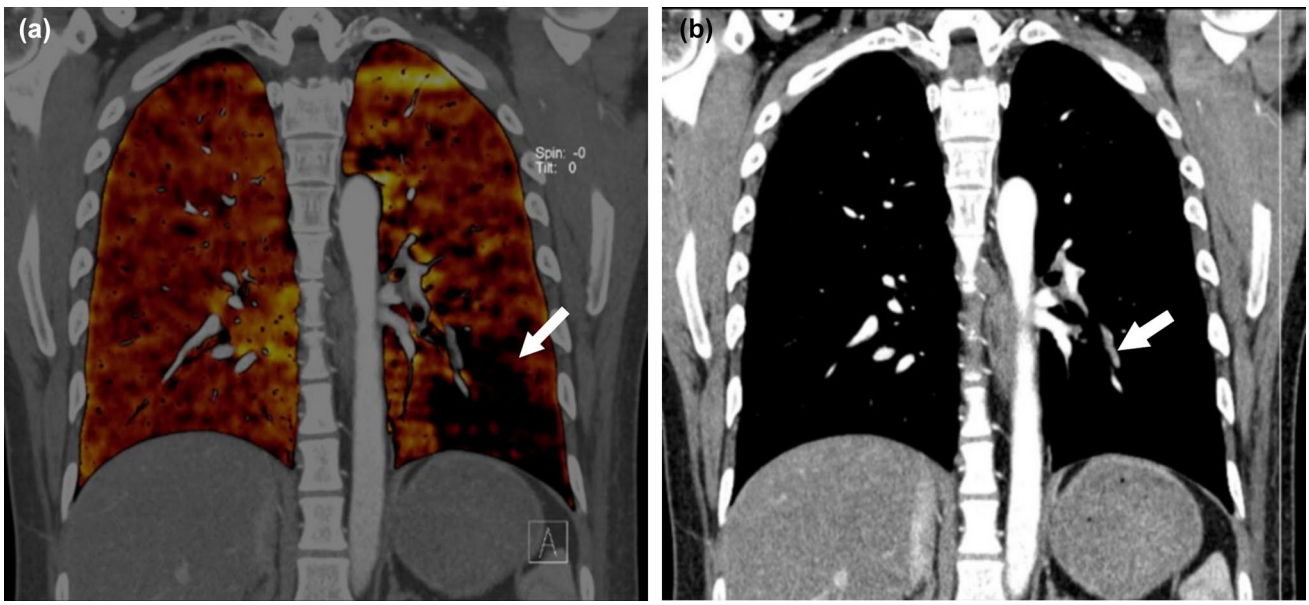

Fig. 5 Acute pulmonary embolism. **a** Coronal PBV map shows a wedge-shaped area of decreased iodine content (arrow) in the left lower lobe. **b** Coronal CT angiography image shows a pulmonary embolus in left lower lobe segmental branch (arrow), which correlates with the perfusion defect shown above

pathology as the reference standard, MECT map was comparable to CTPA with a sensitivity of 100% and a specificity of 98% compared to 100% sensitivity and specificity for CTPA. MECT map was superior to planar perfusion scintigraphy, which had sensitivity of 68% and specificity of 81% [20]. In a small human study with consensus-reading as the reference standard, MECT had a sensitivity/specificity of 76.7/98.2% compared to 85.7/87.5% for SPECT/CT V/Q scintigraphy and 100/100% for CTPA [21].

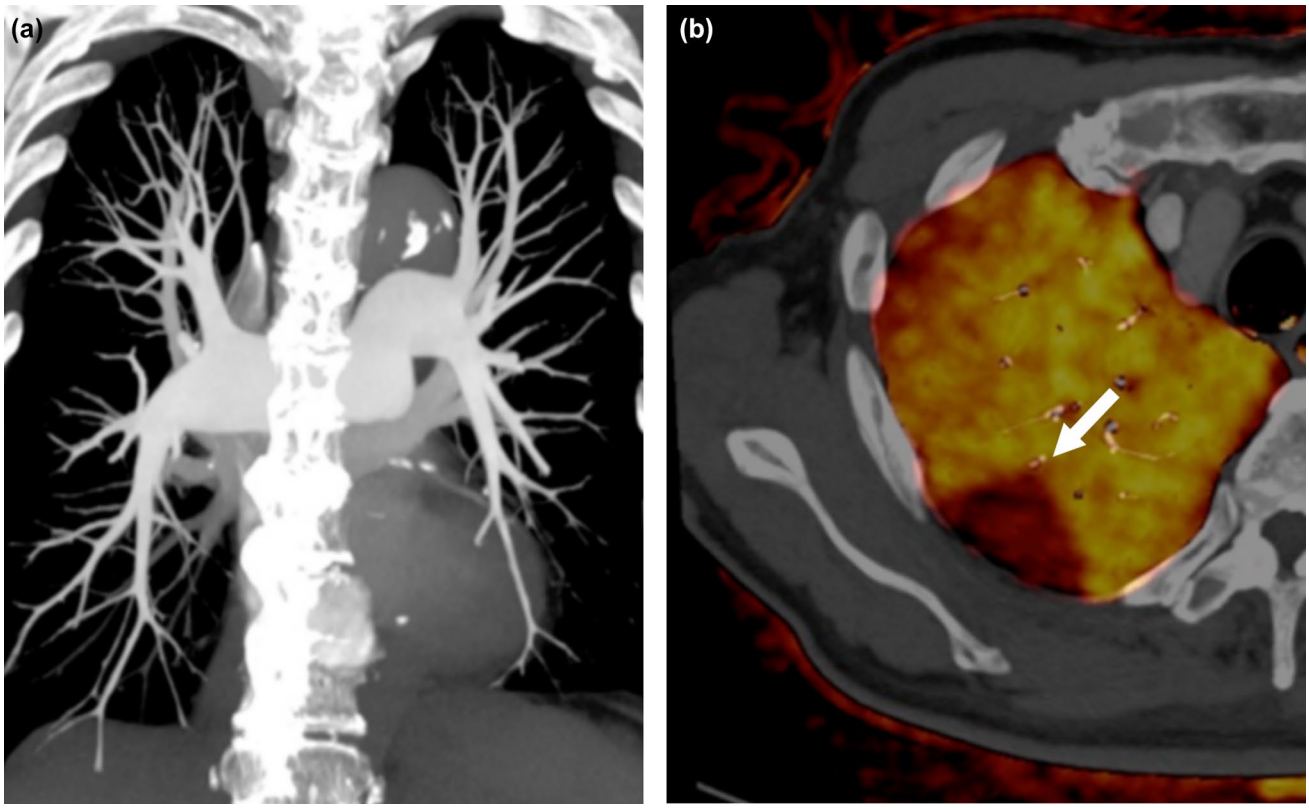

Fig. 6 Acute pulmonary embolism. **a** Coronal MIP reconstruction of CTA shows normal pulmonary arteries without evidence of clot. **b** Axial PBV map shows a wedge shaped perfusion defect (arrow), which is consistent with a perfusion defect from a subsegmental embolism which was not clearly evident in the CTA

A valuable application of MECT is for the detection of small and peripheral PEs which can be missed on CTPA, but manifests with perfusion defects [22] (Fig. 6). This can be the result of a previous PE with re-perfused segmental vessels and residual thrombosis in peripheral vessels that are too small to visualize by CTPA [10, 21, 23], especially in vessels less than 2 mm in diameter [3]. Sometimes, a visible PE may be missed in the initial review of a CTPA, but the presence of perfusion defect in MECT alerts the radiologists to reevaluate the CTPA more carefully for the presence of a small clot [3]. An experimental rabbit study showed that the sensitivity for detection of PE increased in MECT to 89% compared to 67% for CTPA alone, with correct identification of subsegmental PEs [24]. A canine study also showed a sensitivity of MECT of 90% for segmental and 96% for subsegmental and distal PE compared to 89% for CTPA alone [25]. A recent human study showed that with the addition of iodine maps, additional PEs were found in 2.3% of CTs, with all of them being subsegmental (78%) or segmental (22%) and the majority being occlusive (89%) [26]. Overall, 1.0% of patients had a new diagnosis of PE [26]. The management of small PEs is debatable, with some institutions anticoagulating these patients to prevent chronic PEs and their complications. One study showed lower fatality rates of PEs detected with CT than scintigraphy (3.3 vs 5.7%) [27]. However, other studies have shown no fatal outcome in 3 months for untreated isolated subsegmental PEs [28] and minimal improvement in outcome by increased detection of these PEs [29]. Subsegmental PEs may be significant in patients with inadequate cardiopulmonary reserve, coexisting deep vein thrombosis, or thrombophilia [10].

Perfusion defects are not specific for PE and need to be correlated with the lung window of the CT scan to exclude other pulmonary pathologies (emphysema, consolidation, atelectasis, mass, or systemic arterial supply) [30]. Areas with attenuation outside the thresholding values, for example emphysema and ground glass opacities, appear as dark perfusion defects. Artifacts such as motion (cardiac or respiratory) and beam hardening due to dense contrast also cause pseudodefects [30]. Perfusion defects are occasionally not seen in acute PE, typically in non-occlusive clots. In one study, only 5 of 58 non-occlusive clots had corresponding perfusion defects, and in another study, only 2 of 33 non-occlusive clots had perfusion defects [18, 19]. Other studies have shown perfusion defects in only 5–10% of non occlusive PEs [23]. In a recent study, 74.3% of occlusive PEs had

matched defects, whereas only 11.4% of non occlusive PEs had matched defects [26].

In pulmonary infarct, there is a peripheral wedge-shaped area of perfusion defect that is larger than the corresponding abnormality seen in lung windows, whereas in embolus without infarct, there is a perfusion defect without a corresponding parenchymal abnormality [6] (Fig. 7). This can be distinguished from pneumonia, which shows heterogeneous decreased or increased iodine distribution, and atelectasis, which shows homogeneously increased iodine distribution. Additionally, the size of the PBV abnormality and lung parenchymal abnormalities are matched in pneumonia and atelectasis, unlike infarct where PBV abnormalities are larger [6]. Lung abscess and necrotic lesions show no iodine distribution, and tumors show more heterogeneous perfusion [6].

Multi-energy CT perfusion defects can be used to quantify the severity of PEs [31], establish prognosis, and monitor response to therapy. Risk stratification is essential to identify the patients who need more aggressive treatment such as interventional procedures and thrombolysis. The presence of a perfusion defect may be useful in determining the significance of PEs for blood oxygenation and the development of PH [12]. The extent of a perfusion defect directly correlates with right heart strain, clot burden (Qanadli index or Mastora index) [32–34], D-dimer level [35], and troponin I (laboratory parameter for PE severity) [36] and inversely correlates with arterial PaO_2 [36]. A higher incidence of deaths and readmission due to PEs was seen in patients with larger perfusion defects involving more than 5% of the total lung volume [35]. Perfusion defects can also be quantified to distinguish the presence or absence of PEs and estimate the severity of PEs. There is a significant difference of iodine density in the perfusion for normal lung (Mean—1.89 mg/ml), non occlusive perfusion defect (0.83 mg/ml) and occlusive perfusion defect (0.27 mg/ml) [31]. Global quantitative PBV values correlate inversely with adverse prognostic indicators such as Qanadli score (CT obstruction index), RV/LV ratio, troponin I and necessity for ICU admission [37]. A global PBV value of < 60% is associated with a higher occurrence of ICU admission compared to those with higher PBV [37]. However, the added clinical value of quantitative PBV has not been established and is not typically used in routine practice [3]. Perfusion defect extent is also a good marker for monitoring response to therapy, possibly better than clot burden [10]. Complete resolution of a clot and perfusion defect indicates dissolution of PE [3, 31], whereas persistence of a perfusion defect could be due to persistent PEs, partially occlusive emboli, or fragmented emboli [32].

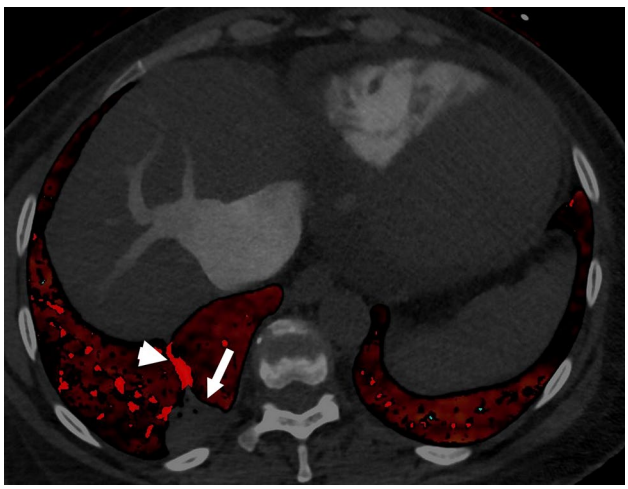

Fig. 7 Pulmonary infarct. Axial PBV map shows a pulmonary infarct in the posterobasal segment of the right lower lobe (arrow), with an embolus in the pulmonary artery (arrowhead) leading to it

Another practical use of MECT in acute PE is the optimization of vascular contrast. MECT provides the option of low energy VMIs (< 70 keV), which have higher contrast due to higher photoelectric attenuation (Fig. 8). This can be used to improve visualization of peripheral arteries and salvage suboptimal studies [38]. Suboptimal studies are not uncommon with CTPAs, due to a variety of reasons including patient and technical factors [39]. Up to 10% of CTPA studies are non-diagnostic, with 40% of these due to poor contrast enhancement [40]. Typically, these patients require a repeat study with an additional bolus of contrast and radiation. Low energy VMIs can increase the vessel attenuation and CNR, thus enabling salvage of a suboptimal study and obviating the need for a repeat injection of contrast. An early study on dual source CT showed that 40 keV VMI had the highest attenuation, SNR and CNR. However, due to higher noise at lower energy levels, 70 keV was found to have the best subjective image quality compared to polyenergetic images [41]. A recent study using dual-layer CT showed that 93% of suboptimally enhanced studies can be salvaged using VMI, with optimal energy levels ranging from 40 to 50 keV. At optimal levels, the improvement of attenuation, SNR and CNR was up to 71%, 63% and 137% [39]. Another study using dual-layer CT showed 99% success in salvaging suboptimal studies, with the highest CNR and diagnostic accuracy seen at 40 keV [42]. This concept can be taken further by using a low dose of intravenous contrast, especially in patients with severe renal dysfunction. A dual source study which used only 35% of the usual iodine concentration showed that 60 keV images had the highest SNR and CNR with maintained image quality [43]. Another dual source study which utilized less than half the iodine load (20 ml vs 50 ml) showed high signal, SNR and CNR at VMI of optimal keV and low noise at 70 keV [44]. High energy VMI can be used to decrease some artifacts, particularly beam hardening artifact emanating from dense contrast in SVC, which can reduce the diagnostic confidence of a CT

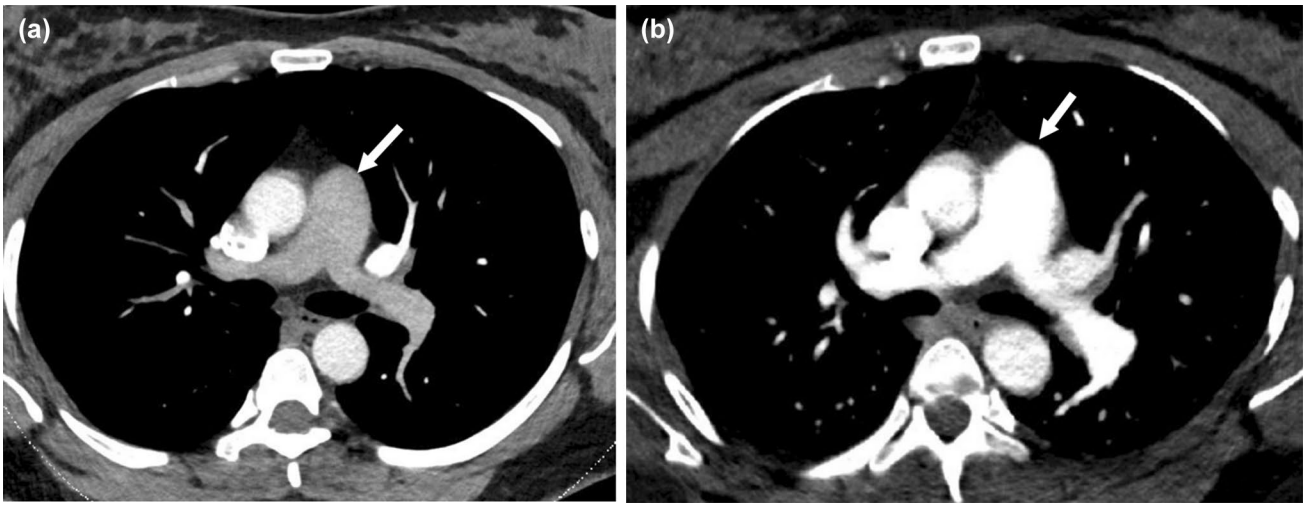

Fig. 8 Boost of contrast in suboptimal studies. **a** Axial CTA image shows suboptimal contrast (mean attenuation-145 HU) in the pulmonary arteries (arrow) which is not adequate for the evaluation of pulmonary embolus. **b** VMI at 40 keV at the same level shows significantly improved contrast (mean attenuation—475 HU) in the pulmonary arteries (arrow), which allows salvage of this suboptimal study without the need for an additional bolus of contrast

scan [1]. The least amount of artifact has been shown at 100 keV [43], with artifact-free analysis of the perivascular anatomic zone without significant difference in image quality compared to 140 kVp [43]. VNC images can be used to evaluate calcification in pulmonary arteries and characterize incidental lesions [1, 3].

Chronic pulmonary embolism

Chronic PE or Chronic thromboembolic disease (CTED) results from obstruction of a pulmonary artery with organized thrombus, causing abnormalities in pulmonary hemodynamics over 6 months or more [45]. The dreaded complication of chronic PE is chronic thromboembolic pulmonary hypertension (CTEPH). In approximately 0.6–9.1% of patients with acute PE, the PE fails to fully resolve and develops into CTEPH within 2 years [45, 46], either due to incomplete resolution of thromboembolus, organized thrombus with intravascular scar, or obstruction and stenosis of peripheral pulmonary arteries due to pulmonary artery remodeling [47, 48]. It is important to diagnose CTEPH since it is a treatable cause of PH. CTPA shows characteristic morphological changes of chronic PE, such as mural detects, webs, bands, intimal irregularities, abrupt stenosis, and complete obstruction [49]. Findings reflecting PH can also be seen, described in the section below. The diagnostic performance of CTPA for detecting CTEPH is high in comparison to invasive pulmonary angiography, particularly at the main/lobar level (sensitivity 95%, specificity 96%) [50, 51] but less so at the segmental level (sensitivity 88%, specificity 89%) [52]. Sensitivity for subsegmental level PEs was 64–70%. In another study, CTPA sensitivity has been shown to be lower than that of V/Q scintigraphy for detecting chronic PEs (51% vs 96–97.4% for V/Q scintigraphy), particularly for peripheral lesions [53], although it is not certain that all the defects seen in V/Q scan are necessarily attributable to CTEPH.

MECT shows perfusion defects in chronic PE, that are typically more extensive than in acute PE. These perfusion defects often appear as well-defined wedge-shaped, mosaic, or mottled areas of decreased iodine content on CT perfusion (Fig. 9). Overall, MECT perfusion has high sensitivity (96–100%) and specificity (76–92%) for the diagnosis of CTEPH [13, 54], and is superior to CTPA which has low sensitivity [55]. With ventilation/perfusion (V/Q) scintigraphic scans as the reference standard, MECT had a sensitivity and specificity of 100% and 92% respectively for detecting chronic PE at the segmental level [54]. Because of this, MECT is a good alternative to V/Q scans for chronic PE and CTEPH, with the additional advantage of obtaining high-resolution morphological information in the same study. Often, a perfusion defect may be the only finding, either due to a small thrombus or recanalization, making this technique extremely valuable in the evaluation of CTEPH [23]. This is particularly relevant in patients who present with chronic dyspnea of unknown etiology.

Perfusion defects from CTED/CTEPH have lower lung attenuation (median: 27 vs 38 Hounsfield units), lower PBV (median: 17 vs 13) and a higher peak pulmonary artery enhancement to lung attenuation ratio (median: 17 vs 11) than acute PE [56]. A delayed phase MECT acquisition shows more enhancement with chronic than acute PE due to the presence of systemic collateral vessels [57]. The pattern of perfusion defect can differentiate CTEPH and idiopathic

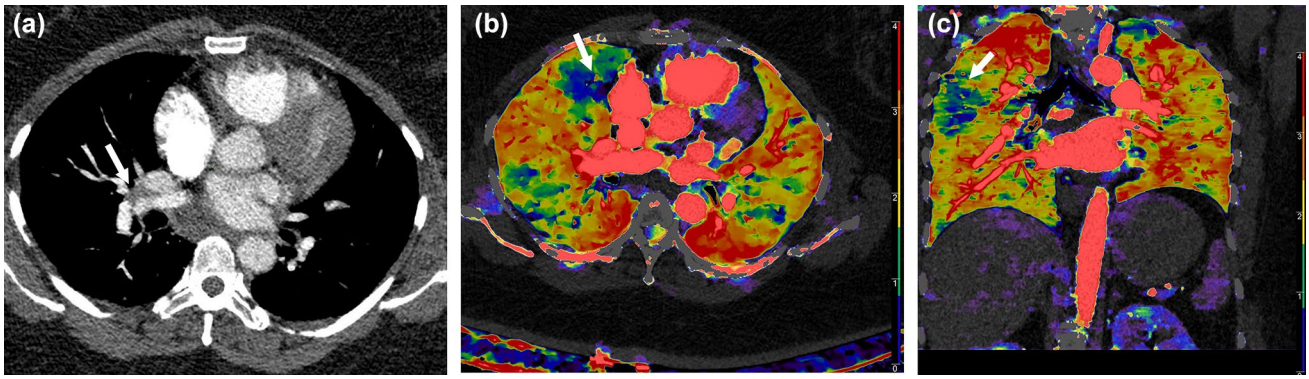

Fig. 9 Chronic pulmonary embolism. **a** Axial CTA shows peripheral filling defect in artery to the right upper lobe (arrow), consistent with chronic pulmonary embolism. **b** Axial CT perfusion image shows heterogeneous perfusion of the entire lung, with a wedge shaped perfusion defect (arrow) color coded as blue in the anterior segment of the right upper lobe. **c** Coronal CT perfusion image shows the wedge shaped perfusion defect in the right upper lobe (arrow)

pulmonary artery hypertension (IPAH) [58]. False positive lesions can be seen due to artifacts and parenchymal lesions [59], making it imperative to evaluate these along with the lung windows of the CT scan. Perfusion defects can also be seen in small airways disease, which also manifests like CTEPH as mosaic attenuation with alternating dark and bright areas. In CTEPH, the perfusion defect is concordant with the dark area of mosaic attenuation, whereas in small airways disease, the perfusion defect is discordant, is usually smaller than the lucent area, and shows air trapping on expiratory imaging [60, 61]. It is also possible to perform a MECT ventilation scan using Xenon gas, which has limited availability and requires careful monitoring [62]. The presence of higher iodine concentration in brighter areas of mosaic attenuation indicates a vascular etiology rather than an airway abnormality [63]. False negative results with normal perfusion in the presence of a chronic PE can be seen due to collateralization or sub-occlusive thrombus, since iodine can pass through collateral vessels unlike perfusion tracers on V/Q scintigraphy [64, 65].

CTEPH is curable by surgery (pulmonary artery endarterectomy [PEA]) or endovascular treatment (balloon pulmonary angioplasty [BPA]) [45, 66–68]. The surgery is successful if it is performed in appropriate patients such as those who have abnormalities at a more proximal level. Hence, if there is a perfusion defect in a segment supplied by a morphologically abnormal and obstructed vessel, it usually responds well to the surgery (Fig. 10). However, a perfusion defect without a corresponding abnormal vessel indicates that the diseases is at a more peripheral level or may reflect a tiny PE that is beyond the limits of spatial resolution of CT. These may not be amenable to surgery [4, 69] and are associated with poor post-procedural results such as persistent elevated mean pulmonary artery pressure (mPAP) and pulmonary vascular resistance (PVR) and higher complication rates [70, 71]. Occasionally, a perfusion defect is absent distal to an abnormal vessel due to collateral vessel formation, which also responds well to surgery [65]. Thus, MECT provides a one-stop evaluation of anatomy and function, rather than performing consecutive V/Q scan and CTPA studies. The number of abnormal perfused lobes correlates with pre-operative PVR [72]. Post-operative PVR correlated negatively with the presence and extent of central thrombi and dilated bronchial arteries in pre-operative CTs, and 60% of patients without visible central thrombi had poor hemodynamic improvement after surgery [72]. Mosaic changes also reflect extensive distal disease and is a poor prognosis for endarterectomy [72]. Preoperative PVR, subpleural densities, and abnormal lung perfusion correlate positively with post operative PVR [72].

MECT allows for quantitatively assessing the severity of CTEPH and treatment effects. Lung PBV is significantly correlated with mPAP and PVR, which are the gold standards for the estimation of severity and prediction of outcome in patients with CTEPH [73]. Lung PBV allows for the quantitative assessment of perfusion improvement after BPA with significant correlation with the improvement of PAP, PVR, and 6-min walking distance [74]. Moreover, it may be more sensitive for the assessment of the treatment effect than V/Q scintigraphy [75].

Pulmonary hypertension

Pulmonary hypertension (PH) encompasses disorders with elevated resting pulmonary arterial pressure ($\geq$ 25 mm Hg at rest). There are five types based on the 2013 WHO classification [76, 77]. CTPA shows several vascular findings, including dilation of the central pulmonary arteries, a sign which can be used to make a diagnosis of PH as well as establish the etiology, described in detail elsewhere [76]. Secondary changes on the heart such as a dilated right ventricle and atrium as well as reduced function can also be

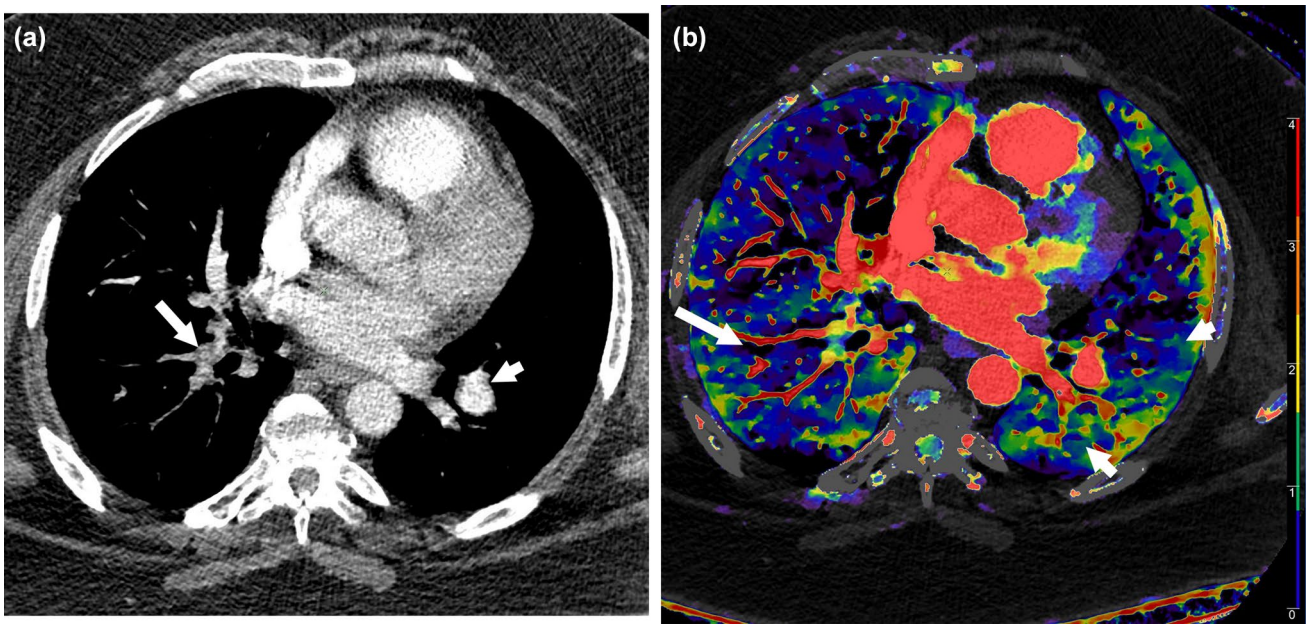

Fig. 10 Chronic pulmonary embolism. **a** Axial CTA image shows that there is an eccentric filling defect in segmental branches of the right lower lobe (arrow), consistent with chronic PE. There is no lesion within left lower lobe segmental branch (arrowhead). **b** Axial CT perfusion image shows heterogeneous perfusion of the lungs, with poor perfusion in the right lower lobe (arrow) which was supplied by the abnormal vessel in CTA, and hence this will have favorable response with pulmonary endarterectomy. There are also perfusion defects in the left lower lobe (arrowheads), which did not have corresponding vascular lesions and hence these will have poor response for surgery

evaluated. The lungs can be assessed for causes of PH and the consequences of PH [76, 78, 79].

In addition to morphological information, MECT also provides functional information on pulmonary perfusion. The changes in CTEPH are described in the section above. Perfusion defects are also seen in non-CTEPH causes of PH due to cellular proliferation, endothelial damage, vasoconstriction, and distal vascular occlusion [80]. Unlike the sharply-defined, large, multiple segmental or subsegmental wedge-shaped defects seen in CTEPH, IPAH shows small, heterogeneous, non-segmental, mottled, and patchy defects [81] (Fig. 11). In PH patients, the attenuation thresholds for PBV are adjusted with the upper limits increased to − 200 or − 300 HU to include areas of the commonly prevalent ground glass opacification in the analysis [3]. Mosaic attenuation pattern of alternating high and lower attenuation areas is seen in the lung parenchymal window settings of the CT scan. Lung window settings are used to distinguish pseudoperfusion defects from parenchymal abnormalities. Vascular mapping is also useful in distinguishing CTEPH from IPAH, with the former having more stenosis and size variations [3].

MECT perfusion defects can be used to assess severity, risk stratification, and prognosis. It also provides insights, both qualitative and quantitative, on pulmonary hemodynamics. Variable correlation has been reported between the absolute pulmonary perfusion quantified in MECT and invasive hemodynamics. Some studies show good correlation with mPAP and PVR [80, 82] whereas other studies did not show correlation [65]. Another parameter that can correlate with PVR is the ratio of central to peripheral pulmonary enhancement. In PH, there is more central than peripheral enhancement [3]. There is also overall decreased global and variable enhancement due to delayed contrast transit [80]. Due to heterogeneous perfusion, regional variation is seen in PBV with high sensitivity, which can be measured manually or automatically and correlates with PVR [80]. PVR is a more accurate indicator of pulmonary vascular disease and can identify patients that may respond to vasodilators [3].

Other uses of MECT in PH include the use of VNC to evaluate for calcification in the vessel wall or calcified thrombi which can be obscured by contrast from CTPA due to recanalization [3, 83, 84]. Right ventricle (RV) myocardial ischemia and delayed iodine enhancement can be evaluated using cardiac CT scans [3]. Low keV VMI can be used to improve visualization of peripheral arteries as well as systemic collateral vessels and can help salvage of suboptimal studies [38].

Miscellaneous

MECT is useful in a few congenital abnormalities and neoplasms. For example, it can be used in the evaluation of lung

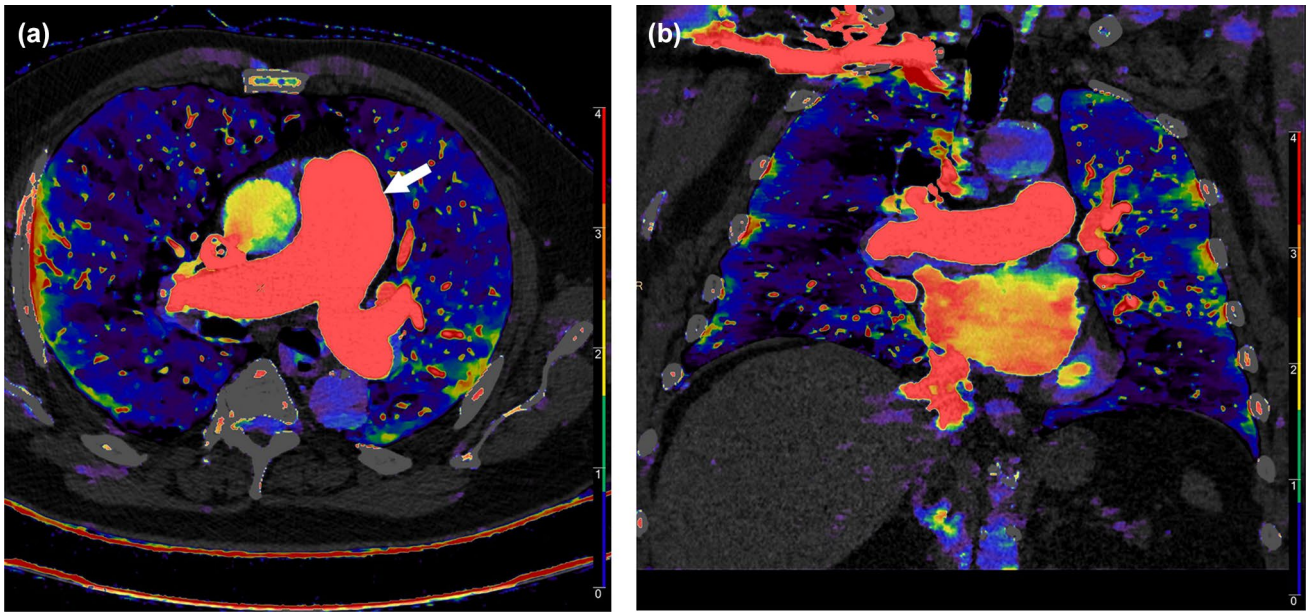

Fig. 11 Pulmonary hypertension. **a** Axial CT perfusion image shows extensive heterogeneous and mottled perfusion (blue color) in a patient with idiopathic pulmonary arterial hypertension. Note that the main pulmonary artery (arrow) is severely dilated, measuring 4.2 cm. **b** Coronal CT perfusion image in the same patient shows heterogeneous perfusion with extensive areas of low perfusion (blue color)

perfusion in congenital disorders. Proximal interruption of the pulmonary artery (agenesis of pulmonary artery) is a congenital absence of either the right or left main pulmonary artery with an intact main pulmonary trunk, usually contralateral to the aortic arch. The lung is usually small, and there is a lot of collateral supply from systemic arteries such as bronchial, internal mammary, brachiocephalic, subclavian or subdiaphragmatic arteries [83, 85]. In a V/Q scan, no perfusion is demonstrated in the affected lung since 99mTc-macroaggregated albumin is trapped in pulmonary capillary bed and cannot reach collateral systemic circulation. However, with MECT, perfusion is demonstrated in the affected lung due to compensatory collateral supply from bronchial and other systemic arteries (Fig. 12), since iodine can pass into the collateral systemic circulation [5]. This can be distinguished from agenesis of lung, in which there is no lung, perfusion, or vascular supply.

Pulmonary arteriovenous malformation (AVM) is a high-flow, low-resistance vascular structure that directly connects a pulmonary artery to a pulmonary vein, bypassing the

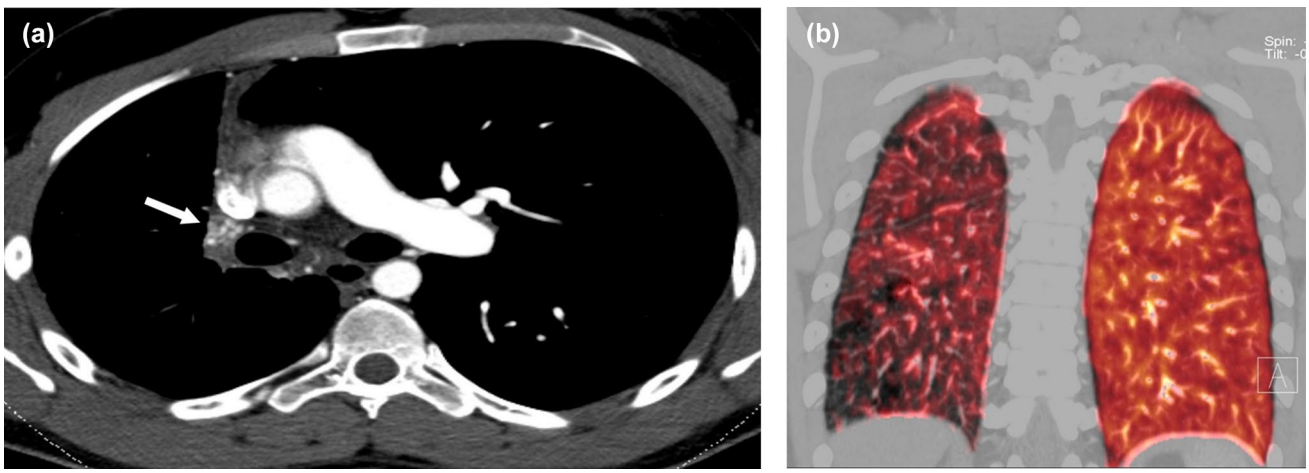

Fig. 12 Pulmonary interruption. **a** Axial CT image shows absence of the right pulmonary artery (arrow), consistent with proximal pulmonary artery interruption. **b** Coronal PBV image of the same patient shows decreased perfusion of the right lung, which is derived from bronchial and systemic collateral circulation

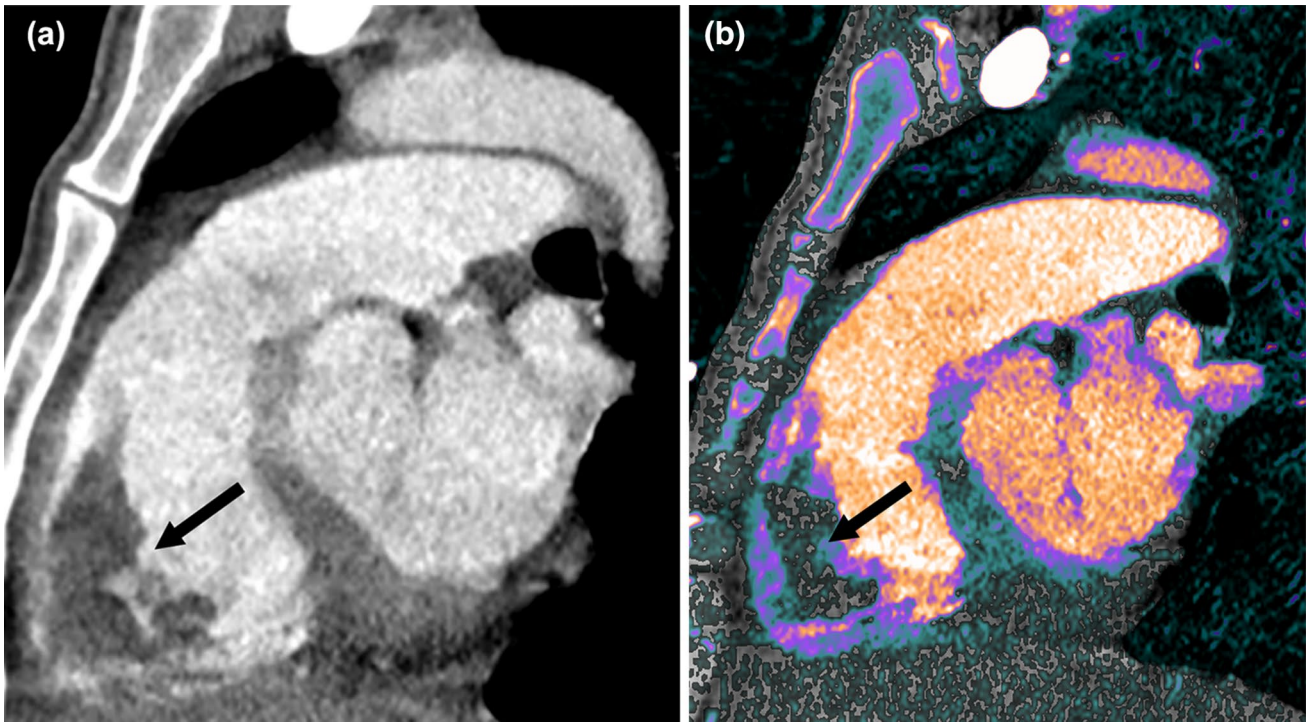

Fig. 13 Mass. **a** Sagittal CT image through the mass shows a large lobulated mass in the apex of the right ventricle (arrow). **b** Iodine map image in the same plane shows that the iodine concentration of the mass (arrow) was 0.1 mg/ml, indicating that this is a thrombus

capillary bed. Majority of the pulmonary AVMs are congenital, commonly seen in hereditary hemorrhagic telangiectasia. On CT angiography, a single feeding artery is connected by a bulbous, non-septated communication to one or more draining veins. MECT may improve that depiction and evaluation of pulmonary AVM. Thin axial and coronal PBV images can demonstrate small AVMs along with their nidi [6]. Mildly increased iodine distribution is seen in the AVM and its nidus compared to pulmonary hemorrhage, scarring or inflammation, which also manifests as ground glass opacity in a conventional CT [6]. One small study showed that a wedged shaped perfusion defect was seen in 40% of cases with pulmonary AVMs, with corresponded to the disease extent [59]. Low-energy VMI can be used to enhance the contrast signal to detect small AVM. VNC can be used to distinguish contrast enhancement from calcification.

MECT is also useful in the evaluation of neoplasms involving the pulmonary vasculature. In particular, it can distinguish a tumor in the pulmonary artery from a bland embolus by evaluating the iodine concentration. Undifferentiated intimal sarcoma is the most common type of pulmonary artery sarcoma which is seen as a mass with irregular margins filling and expanding the lumen of the pulmonary artery [83]. The tumor may spread in the direction of flow, resulting in distal emboli. The presence of contrast enhancement and uptake in FDG-PET helps in distinguishing a sarcoma from PE [83, 86]. Although the attenuation (HU) values of both of these lesions can be similar, in MECT, the tumor shows a higher iodine concentration (1.49 ± 0.57 vs 0.61 ± 0.39) and a higher iodine attenuation value (27.9 ± 9.1 HU vs 10.6 ± 7.2) compared to PE [87] (Fig. 13). One study on rapid kvp switching technology showed that a iodine < 1.74 mg/ml has 100% sensitivity and 100% specificity and area under curve of 1 for diagnosing thrombus [88].

MECT can also be used in the evaluation of vasculitis. Apart from the morphological changes of vessel wall thickening and delayed contrast enhancement, perfusion defects have been reported in the lungs due to involvement of the pulmonary circulation.

Conclusion

MECT iodine maps are highly useful in the evaluation of pulmonary perfusion in acute pulmonary embolism, chronic pulmonary embolism, pulmonary hypertension, congenital abnormalities, neoplasms, and vasculitis. The addition of functional information to morphological information obtained from CTPA makes MECT a one-stop-shop for evaluating pulmonary vascular abnormalities. VMI at low energy levels are utilized to enhance vascular contrast, and VMI at high energy levels are utilized to decrease several artifacts.

Funding The paper did not receive any external or internal funding.

Compliance with ethical standards

Conflict of interest The authors have no conflict of interest or financial disclosure.

Informed consent The study did not include research involving human participants and/or animals and did not require informed consent.

References

1. Kalisz K, Halliburton S, Abbara S et al (2017) Update on cardiovascular applications of multienergy CT. Radiographics 37(7):1955–1974
2. Rassouli N, Etesami M, Dhanantwari A, Rajiah P (2017) Detector-based spectral CT with a novel dual-layer technology: principles and applications. Insights Imaging 8(6):589–598
3. Ameli-Renani S, Rahman F, Nair A et al (2014) Dual-energy CT for imaging of pulmonary hypertension: challenges and opportunities. Radiographics 34:1769–1790
4. Lu GM, Zhao YE, Zhang JL, Schopef JU (2012) Dual-energy CT of the lung. AJR Am J Roentgenol 199:S40–S53
5. Kang MJ, Park CM, Lee CH et al (2010) Dual-energy CT: clinical applications in various pulmonary diseases. Radiographics 30(3):685–698
6. Otrakji A, Digumarthy SR, Gullo RL et al (2016) Dual-energy CT: spectrum of thoracic abnormalities. Radiographics 36(1):38–52
7. Masy M, Giordano J, Petyt G et al (2018) Dual-energy CT (DECT) lung perfusion in pulmonary hypertension: concordance rate with V/Q scintigraphy in diagnosing chronic thromboembolic pulmonary hypertension (CTEPH). Eur Radiol 28(12):5100–5110
8. Kim NH, Delcroix M, Jenkins DP et al (2013) Chronic thromboembolic pulmonary hypertension. J Am Coll Cardiol 62:D92–D99
9. Miles KA (2006) Perfusion imaging with computed tomography: brain and beyond. Eur Radiol 16(Suppl 7):M37–M43
10. Lu GM, Wu SY, Yeh BM, Zhang LJ (2010) Dual-energy computed tomography in pulmonary embolism. Br J Radiol 83:707–718
11. Sokhi HK, Nair A, Ameli Renani SM et al (2011) Quantitative evaluation of dual energy CT (DECT) perfused blood volume (PBV) measurements in a tiered contrast volume cohort [abst]. In: Barr RG (ed) Radiological Society of North America Scientific assembly and annual meeting program. Radiological Society of North America, Oak Brook, p 253
12. Thieme SF, Becker CT, Hacker M et al (2008) Dual energy CT for the assessment of lung perfusion: correlation to scintigraphy. Eur J Radiol 68:369–374
13. Nakazawa T, Watanabe Y, Hori Y et al (2011) Lung perfused blood volume images with dual-energy computed tomography for chronic thromboembolic pulmonary hypertension: correlation to scintigraphy with single-photon emission computed tomography. J Comput Assist Tomogr 35(5):590–595
14. Hess S, Frary EC, Gerke O, Madsen PH (2016) State-of-the-art imaging in pulmonary embolism: ventilation/perfusion single-photon emission computed tomography versus computed tomography angiography—controversies, results, and recommendations from a systematic review. Semin Thromb Hemost 42(8):833–884
15. Moore AJE, Wachsmann J, Chamarthy MR et al (2018) Imaging of acute pulmonary embolism: an update. Cardiovasc Diagn Ther 8(3):225–243
16. Ruzsics B, Lee H, Zwerner PL et al (2008) Dual-energy CT of the heart for diagnosing coronary artery stenosis and myocardial ischemia: initial experience. Eur Radiol 18(11):2414–2424
17. Cai XR, Feng YZ, Qiu L et al (2015) Iodine distribution map in dual-energy computed tomography pulmonary artery imaging with rapid kVp switching for the diagnostic analysis and quantitative evaluation of acute pulmonary embolism. Acad Radiol 22(6):743–751
18. Fink C, Johnson TR, Michaely HJ et al (2008) Dual-energy CT angiography of the lung in patients with suspected pulmonary embolism: initial results. Rofo 180:879–883
19. Thieme SF, Johnson TRC, Lee C et al (2009) Dual-energy CT for the assessment of contrast material distribution in the pulmonary parenchyma. AJR Am J Roentgenol 193(1):144–149
20. Zhang LJ, Chai X, Wu SY et al (2009) Detection of pulmonary embolism by dual energy CT: correlation with perfusion scintigraphy and histopathological findings in rabbits. Eur Radiol 19:2844–2854
21. Thieme SF, Graute V, Nikolaou K et al (2012) Dual energy CT lung perfusion imaging: correlation with SPECT/CT. Eur J Radiol 81(2):360–365
22. Okada M, Kunihiro Y, Nakashima Y et al (2015) Added value of lung perfused blood volume images using dual-energy CT for assessment of acute pulmonary embolism. Eur J Radiol 84:172–177
23. Pontana F, Faivre JB, Remy-Jardin M et al (2008) Lung perfusion with dual-energy multidetector-row CT (MDCT): feasibility for the evaluation of acute pulmonary embolism in 117 concsecutive patients. Acad Radiol 15:1494–1504
24. Zhang LJ, Zhao YE, Wu SY et al (2009) Detection of pulmonary embolism by dual energy CT: an experimental study in rabbits. Radiology 242:61–70
25. Tang CX, Zhang LJ, Han ZH et al (2013) Dual-energy CT based vascular iodine analysis improves sensitivity for peripheral pulmonary artery thrombus detection: an experimental study in canines. Eur J Radiol 82(12):2270–2278
26. Weidman EK, Plodowski AJ, Halpenny DF et al (2018) Dual-energy CT angiography for detection of pulmonary emboli: incremental benefit of iodine maps. Radiology 289(2):546–553
27. Sheh SH, Bellin E, Freeman KD, Haramati LB (2012) Pulmonary embolism diagnosis and mortality with pulmonary CT angiography versus ventilation-perfusion scintigraphy: evidence of overdiagnosis with CT? AJR Am J Roentgenol 198(6):1340–1345
28. Pena E, Kimpton M, Dennie C et al (2012) Difference in interpretation of computed tomography pulmonary angiography diagnosis of subsegmental thrombosis in patients with suspected pulmonary embolism. J Thromb Haemost 10(3):496–498
29. Wiener RS, Schwartz LM, Woloshin S (2011) Time trends in pulmonary embolism in the United States: evidence of overdiagnosis. Arch Intern Med 171(9):831–837
30. Kang MJ, Park CM, Lee CH et al (2010) Focal iodine defects on color-coded iodine perfusion maps of dual-energy pulmonary CT angiography images: a potential diagnostic pitfall. AJR Am J Roentgenol 195(5):W325–W330
31. Wu HW, Cheng JJ, Li JY et al (2012) Pulmonary embolism detection and characterization through quantitative iodine-based material decomposition images with spectral computed tomography imaging. Invest Radiol 47:85–91
32. Zhang LJ, Yang GF, Zhao YE et al (2009) Detection of pulmonary embolism using dual-energy computed tomography and correlation with cardiovascular measurements: a preliminary study. Acta Radiol 50:892–901
33. Chae EJ, Seo JB, Jang YM et al (2010) Dual-energy CT for assessment of severity of acute pulmonary embolism: pulmonary perfusion defect score compared with CT angiographic

obstruction score and right ventricular/left ventricular diameter ratio. AJR Am J Roerntgenol 194(3):604–610
34. Apfaltrer P, Bachmann V, Meyer M et al (2012) Prognostic value of perfusion defect volume at dual energy CTA in patients with pulmonary embolism: correlation with CTA obstruction scores, CT parameters of right ventricular dysfunction and adverse clinical outcome. Eur J Radiol 81(11):3592–3597
35. Bauer RW, Frellesen C, Renker M et al (2011) Dual energy CT pulmonary blood volume assessment in acute pulmonary embolism–correlation with D-Dimer level, right heart strain and clinical outcome. Eur Radiol 21(9):1914–1921
36. Thieme SF, Ashoori N, Bamberg F et al (2012) Severity assessment of pulmonary embolism using dual energy CT: correlation of a pulmonary perfusion defect score with clinical and morphological parameters of blood oxygenation and right ventricular failure. Eur Radiol 22(2):269–278
37. Meinel FG, Graef A, Bamberg F et al (2013) Effectiveness of automated quantification of pulmonary perfused blood volume using dual-energy CTPA for the severity assessment of acute pulmonary embolism. Invest Radiol 48:563–569
38. Godoy MCB, Heller SL, Naidich DP et al (2011) Dual-energy MDCT: comparison of pulmonary artery enhancement on dedicated CT pulmonary angiography, routine and low contrast volume studies. Eur J Radiol 79(2):e11–e17
39. Ghandour A, Sher A, Rassouli N et al (2018) Evaluation of virtual monoenergetic images on pulmonary vasculature using the dual-layer detector-based spectral computed tomography. J Comput Assist Tomogr 42(6):858–865
40. Jones SE, Wittram C (2005) The indeterminate CT pulmonary angiogram: imaging characteristics and patient clinical outcome. Radiology 237:329–337
41. Apfaltrer P, Sudarski S, Schneider D et al (2014) Value of monoenergetic low-kV dual energy CT datasets for improved image quality of CT pulmonary angiography. Eur J Radiol 83(2):322–328
42. Bae K, Jeon KN, Cho SB et al (2018) Improved opacification of a suboptimally enhanced pulmonary artery in Chest CT: experience using a dual-layer detector spectral CT. AJR Am J Roentgenol 210(4):734–741
43. Delesalle MA, Pontana F, Duhamel A et al (2013) Spectral optimization of chest CT angiography with reduced iodine load: experience in 80 patients evaluated with dual-source, dual-energy CT. Radiology 267:256–266
44. Dong J, Wang X, Jiang X et al (2013) Low contrast agent dose dual-energy CT monochromatic imaging in pulmonary angiography versus routine CT. J Comput Assit Tomogr 37:618–625
45. Galiè N, Humbert M, Vachiery JL et al (2016) 2015 ESC/ERS Guidelines for the diagnosis and treatment of pulmonary hypertension: the Joint Task Force for the Diagnosis and Treatment of Pulmonary Hypertension of the European Society of Cardiology (ESC) and the European Respiratory Society (ERS): Endorsed by: Association for European Paediatric and Congenital Cardiology (AEPC), International Society for Heart and Lung Transplantation (ISHLT). Eur Heart J 37:67–119
46. Sueyoshi E, Tsutsui S, Hayahida T et al (2011) Quantification of lung perfusion blood volume by dual-energy CT in patients with and without pulmonary embolism: preliminary results. Eur J Radiol 80(3):e505–e509
47. Galiè N, Kim H (2006) Pulmonary microvascular disease in chronic thromboembolic pulmonary hypertension. Proc Am Thorac Soc 3:571–576
48. Yi ES, Kim H, Ahn H et al (2000) Distribution of obstructive intimal lesions and their cellular phenotypes in chronic pulmonary hypertension. A morphometric and immunohistochemical study. Am J Respir Crit Care Med 162:1577–1586
49. Auger WR, Fedullo PF, Moser KM et al (1992) Chronic major-vessel thromboembolic pulmonary artery obstruction: appearance at angiography. Radiology 182:393–398
50. van der Meer RW, Pattynama PM, van Strijen MJ et al (2005) Right ventricular dysfunction and pulmonary obstruction index at helical CT: prediction of clinical outcome during 3-month follow-up in patients with acute pulmonary embolism. Radiology 235:798–803
51. Reichelt A, Hoeper MM, Galanski M et al (2009) Chronic thromboembolic pulmonary hypertension: evaluation with 64-detector row CT versus digital subtraction angiography. Eur J Radiol 71:49–54
52. Dong C, Zhou M, Liu D et al (2015) Diagnostic accuracy of computed tomography for chronic thromboembolic pulmonary hypertension: a systematic review and meta-analysis. PLoS ONE 10(4):e0126985
53. Pitton MB, Kemmerich G, Herber S et al (2002) Chronic thromboembolic pulmonary hypertension: diagnostic impact of multi-slice CT and selective pulmonary-DSA. Rofo 174(4):474–479
54. Dournes G, Verdier D, Montaudon M et al (2014) Dual-energy CT perfusion and angiography in chronic thromboembolic pulmonary hypertension: diagnostic accuracy and concordance with radionuclide scintigraphy. Eur Radiol 24(1):42–51
55. Tunariu N, Gibbs SJ, Win Z et al (2007) Ventilation-perfusion scintigraphy is more sensitive than multidetector CTPA in detecting chronic thromboembolic pulmonary disease as a treatable cause of pulmonary hypertension. J Nucl Med 48:680–684
56. Nallasamy N, Bullen J, Karim W et al (2018) Evaluation of vascular parameters in patients with pulmonary thromboembolic disease using dual-energy computed tomography. J Thorac Imaging. https://doi.org/10.1097/RTI.0000000000000383
57. Hong YJ, Kim YY, Choe KO et al (2013) Different perfusion patterns between acute and chronic pulmonary thromboembolism: evaluation with two-phase dual-energy perfusion CT. AJR Am J Roentgenol 200:812–817
58. Giordano J, Khung S, Duhamel A et al (2017) Lung perfusion characteristics in pulmonary arterial hypertension (PAH) and peripheral forms of chronic thromboembolic pulmonary hypertension (pCTEPH): dual-energy CT experience in 31 patients. Eur Radiol 27(4):1631–1639
59. Kim BH, Seo JB, Chae EJ et al (2012) Analysis of perfusion defects by causes other than acute pulmonary thromboembolism on contrast-enhanced dual-energy CT in consecutive 537 patients. Eur J Radiol 81(4):e647–e652
60. Bartalena T, Oboldi D, Guidalotti PL et al (2008) Lung perfusion in patients with pulmonary hypertension: comparison between MDCT pulmonary angiography with MiniIP reconstructions and 99 m Tc-MAA perfusion scan. Invest Radiol 43:368–373
61. Hoey ET, Agrawal SK, Ganesh V et al (2009) Dual energy CT pulmonary angiography findings in a patient with chronic thromboembolic pulmonary hypertension. Thorax 64(11):1012
62. Thieme SF, Hoegl S, Nikolaou K et al (2010) Pulmonary ventilation and perfusion imaging with dual-energy CT. Eur Radiol 20(12):2882–2889
63. Pontana F, Remy-Jardin M, Duhamel A et al (2010) Lung perfusion with dual-energy multi-detector row CT: can it help recognize ground glass opacities of vascular origin? Acad Radiol 17:587–594
64. Renard B, Remy-Jardin M, Santangelo T et al (2011) Dual-energy CT angiography of chronic thromboembolic disease: can it help recognize links between the severity of pulmonary arterial obstruction and perfusion defects? Eur J Radiol 79:467–472
65. Hoey ET, Mirsadraee S, Pepke-Zaba J et al (2011) Dual-energy CT angiography for assessment of regional pulmonary perfusion in patients with chronic thromboembolic pulmonary hypertension: initial experience. AJR Am J Roentgenol 196(3):524–532

66. Corsico AG, D'Armini AM, Cerveri I et al (2008) Long-term outcome after pulmonary endarterectomy. Am J Respir Crit Care Med 178:419–424
67. Ishida K, Masuda M, Tanabe N et al (2012) Long-term outcome after pulmonary endarterectomy for chronic thromboembolic pulmonary hypertension. J Thorac Cardiovasc Surg 144:321–326
68. Inami T, Kataoka M, Ando M et al (2014) A new era of therapeutic strategies for chronic thromboembolic pulmonary hypertension by two different interventional therapies; pulmonary endarterectomy and percutaneous transluminal pulmonary angioplasty. PLoS ONE 9:e94587
69. Renapurkar RD, Shrikanthan S, Heresi GA et al (2017) Imaging in chronic thromboembolic pulmonary hypertension. J Thorac Imaging 32:71–78
70. Kreitner KF, Kunz RP, Ley S et al (2007) Chronic thromboembolic pulmonary hypertension: assessment by magnetic resonance imaging. Eur Radiol 17(1):11–21
71. Dartevelle P, Fadel E, Mussot S et al (2004) Chronic thromboembolic pulmonary hypertension. Eur Respir J 23(4):637–648
72. Heinrich M, Uder M, Tscholl D et al (2005) CT scan findings in chronic thromboembolic pulmonary hypertension: predictors of hemodynamic improvement after pulmonary thromboendarterectomy. Chest 127(5):1606–1613
73. Takagi H, Ota H, Sugimura K et al (2016) Dual-energy CT to estimate clinical severity of chronic thromboembolic pulmonary hypertension: comparison with invasive right heart catheterization. Eur J Radiol 85(9):1574–1580
74. Koike H, Sueyoshi E, Sakamoto I et al (2016) Quantification of lung perfusion blood volume (lung PBV) by dual-energy CT in patients with chronic thromboembolic pulmonary hypertension (CTEPH) before and after balloon pulmonary angioplasty (BPA): preliminary results. Eur J Radiol 85(9):1607–1612
75. Koike H, Sueyoshi E, Sakamoto I et al (2018) Comparative clinical and predictive value of lung perfusion blood volume CT, lung perfusion SPECT and catheter pulmonary angiography images in patients with chronic thromboembolic pulmonary hypertension before and after balloon pulmonary angioplasty. Eur Radiol 28(12):5091–5099
76. Goerne H, Batra K, Rajiah P (2018) Imaging of pulmonary hypertension: an update. Cardiovasc Diagn Ther 8(3):279–296
77. Rajiah P (2018) The evolving role of MRI in pulmonary hypertension evaluation: a noninvasive approach from diagnosis to follow-up. Radiology 289(1):69–70
78. Sugiura T, Tanabe N, Matsuura Y et al (2013) Role of 320-slice CT imaging in the diagnostic workup of patients with chronic thromboembolic pulmonary hypertension. Chest 143:1070–1077
79. Raymond TE, Khabbaza JE, Yadav R et al (2014) Significance of main pulmonary artery dilation on imaging studies. Ann Am Thorac Soc 11:1623–1632
80. Ameli-Renani S, Ramsay L, Bacon J (2014) Dual-energy computed tomography in the assessment of vascular and parenchymal enhancement in suspected pulmonary hypertension. J Thorac Imaging 29:98–106
81. Lisbona R, Kreisman H, Novales-Dias JD et al (1985) Perfusion lung scanning: differentiation of primary from thromboembolic pulmonary hypertension. AJR Am J Roentgenol 144:27–30
82. Meinel FG, Graef A, Thierfelder KM et al (2014) Automated quantification of pulmonary perfused blood volume by dual-energy CTPA in chronic thromboembolic pulmonary hypertension. Rofo 186:151–156
83. Goerne H, Chaturvedi A, Partovi S, Rajiah P (2018) State-of-the-art pulmonary arterial imaging—part 2. Vasa 47(5):361–375
84. Castañer E, Gallardo X, Ballesteros E et al (2009) CT diagnosis of chronic pulmonary thromboembolism. Radiographics 29(1):31–50
85. Williams EA, Cox C, Chung JH et al (2010) Proximal Interruption of the pulmonary artery. J Thorac Imaging 34(1):56–64
86. Restrepo CS, Betancourt SL, Martinez-Jimenez S, Gutierrez FR (2012) Tumors of the pulmonary artery and veins. Semin Ultrasound CT MRI 33:580–590
87. Chang S, Hur J, Im DJ et al (2016) Dual-energy CT-based iodine quantification for differentiating pulmonary artery sarcoma from pulmonary thromboembolism: a pilot study. Eur Radiol 26(9):3162–3170
88. Hur J, Kim YJ, Lee HJ et al (2012) Cardioembolic stroke: dual-energy cardiac CT for differentiating of left atrial appendage thrombus and circulatory statis. Radiology 263(3):688–695